



Surface properties and bioactivity of PNIPAM-grafted-chitosan/chondroitin multilayers



Yi-Tung Lu^{a,1}, Pei-Tzu Hung^{a,1}, Kui Zeng^b, Christian Woelk^c, Bodo Fuhrmann^d, Kai Zhang^b, Thomas Groth^{a,d,*}

^a Department of Biomedical Materials, Institute of Pharmacy, Martin Luther University Halle-Wittenberg, Heinrich-Damerow-Strasse 4, 06120, Halle (Saale), Germany

^b Department of Wood Technology and Wood-based Composites, Georg-August-University of Göttingen, Büsingenweg 4, D-37077, Göttingen, Germany

^c Pharmaceutical Technology, Institute of Pharmacy, Faculty of Medicine, Leipzig University, 04317, Leipzig, Germany

^d Interdisciplinary Center of Material Science, Martin Luther University Halle-Wittenberg, D-06099, Halle (Saale), Germany

ARTICLE INFO

Keywords:

Poly(N-isopropylacrylamide)
Chitosan
Chondroitin sulfate
Polyelectrolyte multilayers
Vitronectin adsorption
Stem cell adhesion

ABSTRACT

The thermoresponsive poly(*N*-isopropylacrylamide) (PNIPAM) is widely applied in the biomedical field particularly as thermoresponsive substrate for culture of cells. To be used as a stimuli-responsive coating for cell culture, combining PNIPAM with glycosaminoglycans might be an effective approach to improve its bioactivity. In this study, chitosan is grafted with PNIPAM moieties (PCHI) possessing a cloud point at 31 °C and used as a polycation to fabricate thermoresponsive polyelectrolyte multilayers (PEM) with the bioactive polyanion chondroitin sulfate (CS) at pH 4 by layer-by-layer technique. The *in-situ* investigation by surface plasmon resonance and quartz crystal microbalance with dissipation monitoring confirms that the formation of PEMs with CS can be achieved despite the bulky structure of PCHI at 25 °C. The stability of the PEMs is further improved at physiological pH 7.4 by chemical crosslinking using 1-ethyl-3-(3-dimethylaminopropyl) carbodiimide/*N*-hydroxysuccinimide. Moreover, these PEMs exhibit de-swelling and swelling ability with different surface wettability in response to temperature, which triggers the adsorption and desorption of adhesive protein vitronectin on the PEMs. At 37 °C, the PEMs containing PNIPAM particularly associated with CS terminal layer supports protein adsorption and consequently enhances cell adhesion using multipotent murine stem cells. Overall, due to improved stability, crosslinked PNIPAM-modified biogenic multilayers are cytocompatible and hold great potential as culture substrate for different tissue cells and application in tissue engineering.

1. Introduction

The interaction between biomaterial surfaces and biomolecules like proteins is considered a key factor for subsequent regulation of cell adhesion, proliferation and differentiation and thus relevant for biomedical applications [1]. Surface properties of biomaterials including wettability, charge density, topography, and mechanical properties play profound roles for these biological responses [2–6]. In recent years, functionalization of biomaterials with smart polymers has become an attractive strategy to modulate the surface properties in response to environmental cues such as pH, temperature, light, and others [7]. Among them, poly(*N*-isopropylacrylamide) (PNIPAM) with a lower critical solution temperature (LCST) around 32 °C close to physiological temperature has been

applied as a thermoresponsive and biocompatible surface coating used for the application in tissue engineering, drug delivery and protein separation [8,9]. Below LCST, the hydrated feature is attributed to the dominance of hydrophilic amide groups of PNIPAM which are protein repellent and thus anti-cell adhesive. Above LCST, PNIPAM undergoes coil-to-globular transition dominated by its hydrophobic isopropyl groups leading to dehydration of the polymer that favors protein adsorption and promotes cell adhesion [10]. With this advantage, cell sheet engineering has become a major application to detach complete cell sheets below LCST without using harmful enzymatic digestion that destroy cell-cell and cell-matrix adhesions [9]. Therefore, PNIPAM coated substrata have been used for culture and temperature-based harvesting of stem cells maintaining their differentiation ability for tissue regeneration [11–13].

* Corresponding author. Department of Biomedical Materials, Institute of Pharmacy, Martin Luther University Halle-Wittenberg, Heinrich-Damerow-Strasse 4, 06120, Halle (Saale), Germany.

E-mail address: thomas.groth@pharmazie.uni-halle.de (T. Groth).

¹ These authors contributed equally to this work regarding as the first author.

<https://doi.org/10.1016/j.smaim.2022.11.008>

Received 15 September 2022; Received in revised form 22 November 2022; Accepted 27 November 2022

Available online 12 December 2022

2590-1834/© 2022 The Authors. Publishing services by Elsevier B.V. on behalf of KeAi Communications Co. Ltd. This is an open access article under the CC BY-NC-ND license (<http://creativecommons.org/licenses/by-nc-nd/4.0/>).

However, immobilization of PNIPAM on surface requires a certain thickness to permit cell adhesion at temperatures above LCST (e.g. during cell culture in incubators) [8]. Functionalization of surfaces with PNIPAM can be done by *grafting-to* or direct synthesis on the surfaces among other techniques, which requires costly equipment, sophisticated chemical processes to activate surfaces and use of cytotoxic chemicals (e.g. photo initiators) [8,9]. In the last decades, layer-by-layer (LbL) technique has been established for surface modification based on physical adsorption of polyelectrolytes (PEL) and other macromolecular entities as a straightforward approach to precisely control the thickness of surface coatings. Mostly film formation is driven by the electrostatic interaction between oppositely charged PEL [14]. The physiochemical properties of such polyelectrolyte multilayers (PEMs) can be tuned by the nature of selected polymers and environmental conditions such as temperature, pH and ionic strength [15].

The use of polysaccharides as PEL is typically more preferable for biomedical application because of their high biocompatibility, biodegradability, and can represent or mimic components of human tissue [15]. For example, glycosaminoglycans (GAGs) with numerous negatively charged groups are polysaccharide-based components of extracellular matrix (ECM) and cells. They are perfect candidates for natural and biocompatible PELs [15]. Specially, they are highly bioactive, interacting with ECM proteins and growth factors that play important roles in cell adhesion, and regulation of cell growth and differentiation [16]. Among them, chondroitin sulfate (CS) is frequently used as polyanion for PEM formation to make biomimetic surfaces promoting several cell functions. For instance, the expression of adhesive proteins (e.g. fibronectin) secreted from cells was enhanced during culture on CS containing PEM, along with an enhanced osteogenic and chondrogenic differentiation by controlled release of different morphogens from CS-based PEM [17–19]. Chitosan (CHI) as further example, which is derived from the polysaccharide chitin, is one of the mostly chosen polycations for PEM formation due to its abundance, biocompatibility and antibacterial properties [20]. However, the highly hydrated characteristics and fact that its charge density depends on pH is related to lower cell adhesion when CHI as weak PEL is used for PEM formation [21,22]. Improvement of cell adhesion and bioactivity of such PEM can be achieved by chemical crosslinking processes [17,22].

Since PNIPAM is uncharged, a conjugation of PNIPAM with PELs is required for deposition on the surface through LbL processes. The inherent thermoresponsive property of PNIPAM-modified PEMs has been used for stimuli-responsive controlled release of drugs such as EGF receptor inhibitor or anti COVID-19 drug Favipiravir [23,24]. On the other hand, studies on the use of PNIPAM-modified PEM for tissue engineering are rarely found. A first study on PNIPAM-modified PEM to control cell adhesion/detachment was reported by Liao et al. [25]. They prepared PNIPAM film by assembling PNIPAM copolymers with cationic allylamine hydrochloride segment and with anionic styrene sulfonic acid segment. The cationic moiety on the outermost surface seemed to promote FN adsorption that was secreted from cells and further cell adhesion. Although there are a few studies about protein adsorption on PNIPAM-based PEMs using ovalbumin, structure and properties of PNIPAM-modified PEM related to protein adsorption and cell behavior remain still to be further elucidated [26,27].

In this study, we establish a protocol to modify CHI covalently with PNIPAM (referred as PCHI) studying its thermoresponsive properties and applicability to serve as polycation for making thermoresponsive PEM with CS as bioactive polyanion. The effect of the presence of bulky PNIPAM on growth behavior, thickness, viscoelastic and surface properties of PEM are investigated with physical methods. An attempt to increase stability and cell-adhesive properties of PEM under physiological conditions is done by covalent crosslinking. In particular, crosslinking and terminal layer composition like CHI and PCHI versus CS are supposed to affect adsorption of adhesive (extracellular matrix) proteins and adhesion of cells. Thus, these factors are analyzed towards adsorption of the cell-adhesive protein vitronectin, as well as cytocompatibility,

including the study of adhesion and growth of the multipotent mouse fibroblast cell line C3H10T1/2 as a general model for culture of stem cells that is interesting for applications in regenerative medicine.

2. Materials and methods

2.1. Materials

Chitosan (CHI, deacetylation $\geq 92.6\%$, Mw = 40–150 kDa) was purchased from HMC Heppe Medical Chitosan GmbH (Halle, Germany). Chondroitin sulfate A (CS) from the bovine trachea (Mw ~ 25 kDa) was provided by Sigma-Aldrich (Steinheim, Germany). Carboxylic acid-terminated PNIPAM (PNIPAM-COOH, Mw = 10 kDa), *N*-hydroxysuccinimide (NHS), polyethylene imine (PEI, Mw ~ 750 kDa) and fluorescein isothiocyanate (FITC) were purchased from Sigma-Aldrich (Steinheim, Germany). Tetrahydrofuran (THF) and *n*-hexane were provided by Th. Geyer GmbH & Co. KG (Renningen, Germany). 1-ethyl-3-(3-dimethylaminopropyl) carbodiimide (EDC) were obtained from Thermo Fisher (Kandel) GmbH (Karlsruhe, Germany). Recombinant human vitronectin (VN) was from PeproTech, Inc. (Hamburg, Germany).

2.2. Synthesis of thermoresponsive PNIPAM-grafted-CHI

PNIPAM-grafted-CHI (PCHI) synthesis has been described in more detail elsewhere [28–30]. Briefly, a weight ratio of 1:3 of chitosan and PNIPAM-COOH were separately dissolved in 2% acetic acid. The PNIPAM-COOH aqueous solution was activated by EDC and NHS for 1 h at 25 °C and mixed with the chitosan solution afterwards. The molar ratio based on the repeating unit of chitosan/EDC/NHS molar was 1: 3: 1.5. The mixture was left to react and stirred overnight at 25 °C. After the reaction, precipitation of the product was obtained in a THF/hexane solution (4:1) for 2 times. Finally, the precipitant was purified by dialysis using a membrane with molecular weight cut off (MWCO): 12–14 kDa against Milli-Q water followed by lyophilization with a freeze dryer (ALPHA 1–2 LDplus, Christ, Osterode am Harz, Germany).

The zeta potential measurements were done by laser Doppler velocimetry using a Zetasizer Nano ZS ZEN3600 (Malvern Instruments Ltd., UK) and a clear disposable folded capillary cell (DTS1060, Malvern Instruments). Since high concentration of salt can cause degradation of the electrodes and inaccurate measurement, CS, CHI, and PNIPAM-CHI were prepared at low concentration of 0.5 mg mL⁻¹ in 20 mM NaCl solution at pH 4. Three measurements of 20 cycles were performed under the Smoluchowski approximation with a voltage of 50 V at 25 °C (Zetasizer software 7.12) [31]. The viscosity of 0.8872 mPa s, dielectric constant of 78.5 F/m and refractive index of 1.33 were assumed.

Dynamic light scattering (DLS) was performed with a Zetasizer Nano ZS ZEN3600 (Zetasizer Nano ZS, Malvern Instruments Ltd., UK) using a 5 mW laser with the incident beam of 633 nm (He–Ne laser). To align the conditions of further multilayer process, PCHI was prepared at a concentration of 1 mg mL⁻¹ in 150 mM NaCl solution, pH 4. The hydrodynamic diameter and polydispersity index (PDI) of PCHI were determined in the temperature range of 20–38 °C. Each measurement with 15 runs was done in triplicate and the average was calculated for plotting the results.

2.3. Cleaning of substrates

Silicon wafers (Silicon materials, Kaufering, Germany) and round glass cover slips (\varnothing 12 mm, Menzel, Braunschweig, Germany) were cleaned using a solution of 35% H₂O₂, 25% NH₄OH, and Milli-Q water (1:1:5, v/v/v) at 80 °C for 15 min. Thereafter, the samples were rinsed repetitively with Milli-Q water (6 \times 5 min) and dried with a nitrogen stream. The gold-coated glass sensors (10 \times 10 mm²) for surface plasmon resonance (SPR) (IBIS Technologies B.V., Enschede, The Netherlands) and quartz chips (Au/Ti, 10 MHz) for quartz crystal microbalance with dissipation monitoring (QCM-D) (qCell T, 3t Analytik, Tuttlingen,

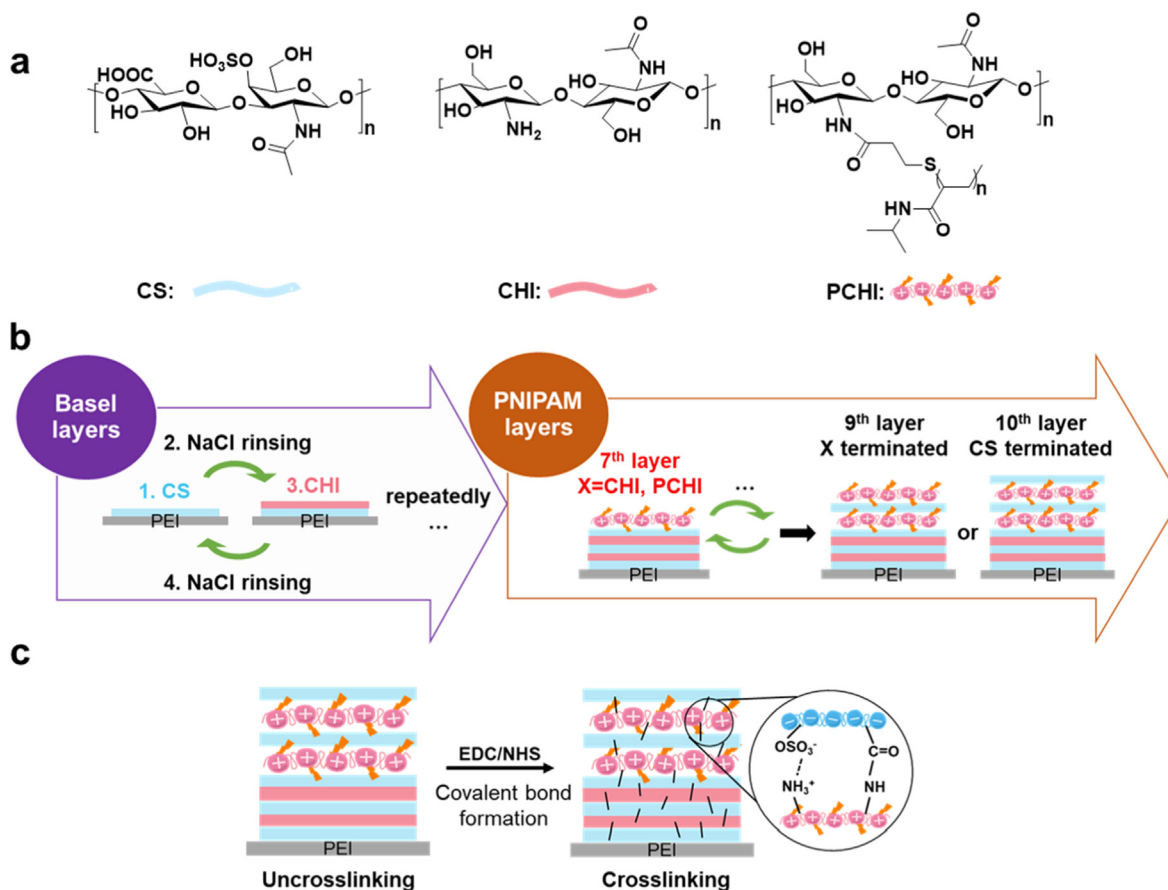


Fig. 1. (a) Molecular units of polymers used in the polyelectrolyte multilayer (PEM) buildup: chondroitin sulfate (CS) as polyanion, chitosan (CHI) and PNIPAM-grafted-chitosan (PCHI) as polycations. (b) Schematic representation for preparation of PCHI-PEM using the layer-by-layer (LbL) technique. The substrate was coated with positively charged polyethylene imine (PEI) as an anchoring layer followed by subsequent CS and CHI adsorption. CHI was replaced by PCHI from 7th layer. (c) Crosslinking of the PEM using EDC/NHS to form amide bonds between CHI or PCHI and CS.

Germany) were gently cleaned with 99% ethanol and Milli-Q water followed by drying with nitrogen.

2.4. Preparation of multilayers with layer-by-layer technique

The PEMs were fabricated on silicon wafers, gold-coated glass sensors, polystyrene well plates, or glass cover slips for SPR, QCM, ellipsometry, water contact angle and biological experiments. The used PELs and assembly procedure of PEM are illustrated in Fig. 1a and b. All PELs were dissolved in 150 mM NaCl solution at a concentration of 1 mg mL^{-1} . CHI was solubilized in 150 mM NaCl solution containing 0.05 M acetic acid at 50°C for 3 h and stirred overnight. The pH of all polyelectrolyte solutions was set at pH 4. All solutions were filtered through a $0.2 \mu\text{m}$ pore size membrane (Whatman). Considering mobility of PNIPAM chain is restricted inside PEM in response to temperature [32,33], here PCHI was only deposited at the outermost region of the entire PEM. An initial anchoring layer of PEI was deposited on the substrate to obtain a positively charged surface which enables strong bonding of PEM to the different substrates. By alternating adsorption of CS as polyanion and CHI as polycation, the basal PEM were built up to 6 total layers. For the PCHI-PEMs, CHI was replaced by PCHI from 7th layer for following deposition step until reaching total number of 9 or 10 layers, where either PCHI or CS was the final layer of PCHI-PEM, respectively. The CHI-PEM system only composed of CHI and CS was referred as comparisons. PEMs with different compositions were named as B-[X/CS]_{1.5} (X-terminated layer) and B-[X/CS]₂ (CS-terminated layer). ‘B’ refers to basal layers from 1–6 layers and ‘X’ is CHI or PCHI.

After PEM formation, the crosslinking was performed with 50 mg

mL^{-1} EDC and 11 mg mL^{-1} NHS in 150 mM NaCl solution at pH 5 (Fig. 1c) according to the protocol described previously [4,22]. PEMs were immersed in the crosslinking solutions and incubated at 4°C for 18 h with gentle shaking. Afterwards, the crosslinking reaction was stopped by washing the samples 3 times with 0.15 M NaCl, pH 8 for each 1 h to remove unreacted EDC/NHS.

2.5. Measurement of multilayer growth

The layer growth and PEM formation were studied at 25°C using surface plasmon resonance (SPR, IBIS Technologies B.V., Enschede, The Netherlands) and quartz crystal microbalance with dissipation monitoring (QCM-D, qCell T, 3t Analytik, Tuttlingen, Germany). In SPR measurement, a shift in the angle (m°) is observed upon the binding of molecules at the gold-liquid interface of the gold coating sensor due to the change of refractive index [34]. The cleaned gold sensor was fixed in the flow chamber and mounted in the SPR device. To begin the measurement, PEI was first introduced to the flow cell and followed by a rinsing step with alternating injection of CS, CHI and PCHI to achieve 10 layers. Each adsorption step of 1 mg mL^{-1} polyelectrolyte solution at pH 4 was 15 min and the rinsing steps using 150 mM NaCl, pH 4 to remove unbound polyelectrolyte was 3×4 min. The mean angle shift (m°) was calculated from 10 values after rinsing obtained from IBIS SPR software 2.1.21 for plotting the graph of layer growth.

QCM-D technique was performed to quantify the adsorbed ‘acoustic’ mass including solvent that is associated with the PEM as well as the damping shift caused by the PEM on the sensor. A piezoelectric AT-cut gold-coated quartz sensor can be excited to resonance by applying an

alternative voltage. The resonance frequency of an oscillating quartz crystal is correlated to the mass of the crystal and thus any mass change from adsorbed or desorbed mass leads to a frequency shift. The Sauerbrey model states a linear relationship between the changes in frequency and mass estimated for a thin, rigid and evenly distributed film when there is no change in dissipation [35]. However, when a polysaccharide-based film with high water content is deposited on the surface, the oscillation of resonator is damped by the adsorbed layer. The Kelvin–Voigt model explains the frequency and energy dissipation changes (Δf and ΔD) related to film viscoelastic properties and thickness [36]:

$$\frac{\Delta f}{f} = -\frac{d_f \rho_f}{d_q \rho_q} \left(1 - \eta_0 \eta_0 \times \frac{\left(\frac{\eta_f}{\rho_f} \right) \omega^2}{\mu_f^2 + \omega^2 \eta_f^2} \right) \quad (1)$$

$$\Delta D = -\frac{d_f}{d_q \rho_q} \left(\eta_0 \rho_0 \times \frac{\mu_f \omega^2}{\mu_f^2 + \omega^2 \eta_f^2} \right) \quad (2)$$

where $\omega = 2\pi f$ is the angular frequency of oscillation, d_q and ρ_q are the thickness and density of the quartz crystal resonator. η_0 and ρ_0 are bulk viscosity and density. While d_f and ρ_f are known parameters in the QCM-D device and used in the software, d_f , ρ_f , η_f , and μ_f are the thickness, density, viscosity, and shear modulus of adsorbed film. The viscoelastic thickness of the film can be calculated by fitting the changes of Δf and ΔD in the software. (qGraph Viewer 1.8). The liquid viscosity and density were assumed to be close to water with parameter values of 0.89 Pa s and 0.997 g cm⁻³. The film density was fixed at 1.05 g cm⁻³ based on previous QCM studies on PEM made of polysaccharides [37].

To perform the LbL film build-up, the cleaned quartz gold sensor was placed in the QCM measuring device. A continuous flow at 60 $\mu\text{L min}^{-1}$ was used for all polyelectrolyte deposition with a concentration of 1 mg mL⁻¹ in 150 mM NaCl, pH 4 to reach equilibrium state for 15 min. Rinsing steps using 150 mM NaCl solution at pH 4 were done for 12 min after each layer deposition. The Voigt thickness was automatically calculated from qGraph Viewer 1.8 software based on F and D shifts.

2.6. Effect of temperature on multilayer mass measured by QCM-D

Frequency shifts of the sensor coated with PEM dependent on temperature were monitored using the QCM-D device equipped with a heating chamber. The PEM-coated sensor was mounted in the device and equilibrated with 150 mM NaCl solution at pH 4 or 7.4 at 20 °C with a flow rate = 60 $\mu\text{L min}^{-1}$ for 10 min. Subsequently, the heating process was started in the device for 1 h. After the temperature reached 40 °C, the cooling process ran for another 1 h to reach 20 °C. The heating-cooling cycle was carried out with 0.33 °C min⁻¹ steps.

2.7. Multilayer thickness and hydration degree

The dry thickness of uncrosslinked and crosslinked multilayers was measured by spectroscopic ellipsometry (M – 2000V, J.A. Woollam Co., Lincoln, NE, USA) in the wavelength range of 375–1000 nm at 25 °C. The spectroscopic scan was at the range of angles from 51° to 60°. A cleaned Si wafer coated with SiO₂ layer was used as the reference. In addition, the layer thickness was used to examine the stability of PEMs by rinsing with phosphate buffered saline (PBS, pH 7.4, Biochrom AG, Germany) followed by Dulbecco's modified Eagle's medium (DMEM, pH 7.4, HiMedia Laboratories Pvt. Ltd., Germany) and dried with a nitrogen stream. The measurements were done two times on different locations of each PEM surface with duplicate measurements. The thickness was obtained using the WVASE32 software applying Cauchy model [38]. In addition, the hydration degree was calculated by dry thickness and viscoelastic thickness from ellipsometry and Voigt model using equation (3):

$$\text{Hydration \%} = \frac{\text{Thickness (Voigt - Ellipsometry)}}{\text{Thickness (Voigt)}} \quad (3)$$

2.8. Surface wettability of multilayers

Static water contact angle measurement for studying surface wettability of the terminal layers was carried out by OCA 15+ system (Data-Physics GmbH, Filderstadt, Germany) with a heating element. The sessile drop method was performed on the multilayer surfaces first at 20 °C and then at 37 °C. The volume of 1 μL Milli-Q water was dispensed on the surface with a flow rate of 0.5 $\mu\text{L s}^{-1}$. Ellipse fitting was chosen as the preferred fitting method to calculate the water contact angles (WCA). Each sample was measured at least 10 times at different positions to calculate average value and standard deviation.

2.9. Biological investigations

2.9.1. Protein adsorption and desorption

Fluorometry (FLUOstar Optima, BMG LabTech., Offenburg, Germany) was used to quantify protein adsorption and desorption. FITC-labeled VN (FITC-VN) was prepared according to the protocol for protein labelling (Sigma-Aldrich) as shown in supporting information. Crosslinked PEMs were prepared in black 96-well tissue culture plates (Greiner). The PEM were coated with 70 μL of 5 $\mu\text{g mL}^{-1}$ FITC-VN and incubated at either 25 °C or 37 °C for 1 h. Thereafter, the supernatant of each well was transferred to a new black 96-well plate. The fluorescence intensity of the supernatant was measured to determine the concentration of remaining FITC-VN at an excitation wavelength of 488 nm and an emission wavelength of 530 nm. The fluorescence intensities of known concentrations (0.005, 0.05, 0.1, 0.5 and 5 $\mu\text{g mL}^{-1}$) of FITC-VN were measured to generate a calibration curve for calculation of the amount of adsorbed VN on the surface (indirect estimation).

After removal of FITC-VN supernatants, the PEMs were rinsed with 70 μL PBS (at 4 or 37 °C, pH 7.4) 3 times to remove excess of protein solution. Desorption of VN was conducted by applying 70 μL PBS to the samples which were incubated at 4 °C or 37 °C for 24 h, followed by incubation with 70 μL of 200 mM NaOH at 37 °C for another 2 h. The PBS and NaOH supernatants were collected and the fluorescence intensity measured to determine the amount of desorbed FITC-VN.

2.9.2. Cell culture

C3H10T1/2 embryonic fibroblasts (Clone 8) were purchased from ATCC (CCL-226, LGC Standards GmbH Wesel, Germany) and cultured in DMEM supplemented with 10% (v/v) fetal bovine serum (FBS, Biochrom AG, Berlin, Germany) and 1% (v/v) antibiotic solution (penicillin/streptomycin, Biochrom AG, Berlin, Germany) at 37 °C in a humidified 5% CO₂/95% air atmosphere using a NUAIRE DH Autoflow incubator (Plymouth, Minnesota, USA). Prior to confluence, cells were harvested from the flask using 0.25% trypsin/0.02% EDTA (Biochrom AG, Berlin, Germany) solution for 5 min at 37 °C. The trypsin was neutralized with DMEM containing 10% FBS +1% Pen/strep. After centrifugation of the cell suspension for 5 min at 500 g, the supernatant was aspirated, and the cell pellet was resuspended in DMEM with 10% FBS +1% Pen/strep. Cells were counted manually using a Neubauer chamber.

2.9.3. Cell viability, adhesion, and growth

The crosslinked PEMs prepared in 24 well tissue culture polystyrenes (TCPS, Greiner, Frickenhausen, Germany) were sterilized by ultraviolet light at 254 nm for 30 min and rinsed twice with sterile PBS. Afterwards, the modified substrates were pre-incubated with DMEM containing 1% Pen/strep at 37 °C for 1 h to deactivate any unreacted EDC/NHS after PEM crosslinking. Then, C3H10T1/2 cells were seeded on PEMs at a cell density of 10⁴ cells per well in serum-containing DMEM (10% FBS+1% Pen/strep) and incubated at 37 °C/5% CO₂/95% air atmosphere.

Cell viability was determined after 24h cultivation by using a

Table 1
Zeta potentials of PEL and degree of substitution (DS) of PNIPAM-grafted-CHI.

Sample	Chitosan: PNIPAM [a]	DS _{PNIPAM}	Zeta potential (mV) [b]
PNIPAM-grafted-chitosan (PCHI)	1:3	0.03	30.7 ± 0.5
Chitosan (CHI)			33.8 ± 0.6
Chondroitin sulfate (CS)			-20.1 ± 1.8

^a Weight ratio of chitosan and PNIPAM during synthesis.

^b Measured at 0.5 mg mL⁻¹ of PEL, at pH 4 in 20 mM NaCl.

fluorescence-based Live/Dead assay with calcein AM and EthD-III (Biotium, Hayward, CA). The cells were rinsed once briefly in Dulbecco's phosphate-buffered saline (DPBS) containing 1 g L⁻¹ glucose. The staining solution containing 2 μM calcein AM (green) and 4 μM EthD-III (red) was added into each well and incubated in the dark for 30 min at 37 °C. Subsequently, the PEM samples were washed with DPBS (Lonza Group Ltd, Bornem, Belgium) containing 1 g L⁻¹ glucose twice and analyzed through a set of an Ar 488 nm laser and He-Ne 543 nm laser using confocal laser scanning microscopy (Carl Zeiss Micro-Imaging GmbH, Jena, Germany) at 37 °C and 5% CO₂. Cell photographs were taken with 10× objectives. Images were processed with the ZEN software (Carl Zeiss). The quantification of cell number, area and aspect ratio were calculated from five images per sample using software Image J.

2.10. Statistical analysis

All statistical analysis was performed with Origin 2019 software. Mean, standard deviation, and analysis of significance were calculated through a one-way ANOVA followed by posthoc Tukey's test (indicated as *). A value of $p < 0.05$ was considered as significantly different. Furthermore, box-whisker diagrams are shown where appropriate. The

box indicates the 25th and 75th percentiles, the median (dash), and the mean value (black square), respectively.

3. Results and discussion

3.1. Synthesis and thermoresponsive properties of PNIPAM-grafted-chitosan (PCHI)

To obtain thermoresponsive PCHI, PNIPAM-COOH was conjugated to chitosan as presented in Fig. S1a PCHI with the degree of substitution (DS) of 0.03 obtained when a ratio of CHI/PNIPAM-COOH of 1:3 (w/w) was applied as listed in Table 1. Based on ¹H NMR spectrum, the calculation of DS of PCHI is described in the supplementary data (Fig. S1b). A further increase of DS of CHI was not possible by increasing PNIPAM concentration, reaction time and temperature despite some findings of other groups. We assume that steric hindrance by the bulky PNIPAM molecule and CHI conformation reduces the number of amino groups along the CHI polymer accessible for *grafting-to*. Because the PEM formation depends on ion pairing between the oppositely charged PELs, the charge density of PELs affects the multilayer formation, as well as the structure and physiochemical characteristics of PEMs [14]. Zeta potential reflects the types of ionic species and the number of charges [39]. As shown in Table 1, CHI has a positive zeta potential value of 33.8 ± 0.6 mV, while the zeta potential of PCHI is slightly lower with 30.7 ± 0.5 mV. The decrease in potential for PCHI is due to the modification of a part of the primary amino groups of CHI with uncharged PNIPAM. In contrast, the zeta potential of the strong polyanion CS is -20.1 ± 1.8 mV (Table 1). Overall, even though the zeta potential is slightly reduced for PCHI, it may be possible to be used as a polycation for PEM formation with CS.

DLS technique is a representative method to analyze the hydrodynamic diameter and polydispersity index (PDI) of thermoresponsive polymers [40–43], here the temperature effect on PCHI was investigated

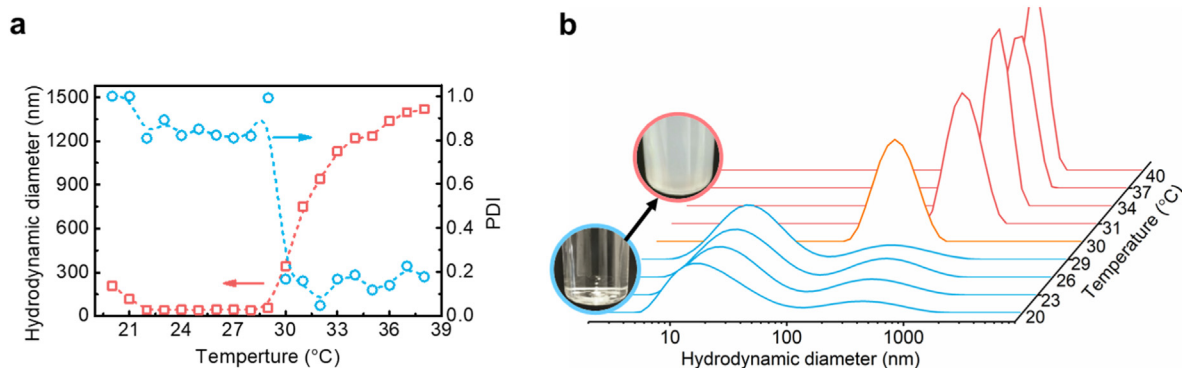


Fig. 2. Dynamic light scattering analysis of PNIPAM-grafted-CHI at a concentration of 1 mg mL⁻¹, pH 4 in 150 mM NaCl aqueous solution in the temperature range from 20 to 39 °C. (a) Hydrodynamic diameter (red line) and PDI (blue line). (b) Size distribution and status of solution below (transparent) and above (opaque) T_{CP}.

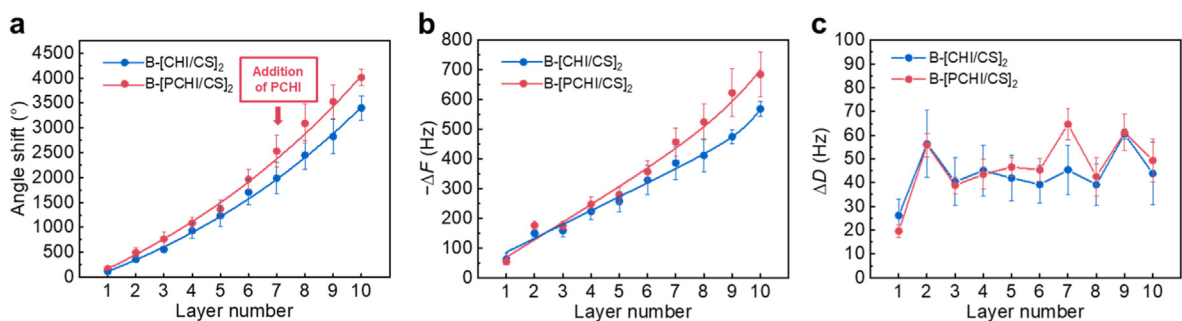


Fig. 3. Layer growth of B-[CHI/CS]₂ and B-[PCHI/CS]₂ PEMs measured from (a) angle shifts by surface plasmon resonance, and (b) frequency shift $-\Delta F$ and (c) damping shift ΔD by QCM-D measurements as a function of layer number. B-[CHI/CS]₂ composed of CS and CHI as a reference. [1–10; 1 = PEL, all even numbers = CS. For odd numbers, the 3rd and 5th = CHI while 7th and 9th = PCHI.] $n = 20$, means ± SD.

Table 2

Comparison of dry thickness (from ellipsometry) and hydrodynamic thickness (from Voigt model) of PEMs. The hydration degree was obtained according to equation (3).

Thickness (nm)	CHI/PCHI-terminated			CS-terminated		
	Ellipsometry	Voigt	Hydration	Ellipsometry	Voigt	Hydration
B-[CHI/CS]	14.8 ± 0.6	17.8 ± 0.3	16.9%	18.8 ± 1.2	19.8 ± 0.8	10.1%
B-[PCHI/CS]	16.4 ± 1.1	22.9 ± 3.9	28.4%	17.9 ± 0.4	24.0 ± 1.3	25.4%

as shown in Fig. 2a. According to recent studies [44], the cloud point temperature (T_{CP}) stands for the phase transition temperature at a specific concentration, whereas the LCST is the lowest temperature in the phase diagram with the full composition range. Therefore, the T_{CP} of PCHI prepared at a concentration of 1 mg mL^{-1} , pH 4 in 150 mM NaCl can be determined by the midpoint of the increasing hydrodynamic diameter [20].

Starting from 20°C , the size of PCHI dramatically changed from the average 40–1200 nm when heating across T_{CP} , which was confirmed at 31°C . In addition, PDI of PCHI was close to 1.0 at lower temperature, while the value decreased to below 0.2 above T_{CP} . PDI measured by DLS represents the size distribution corresponding to Fig. 1b [45]. At low

temperature, the hydrogen bonds between the hydrophilic group and water make PCHI soluble in the aqueous solution (transparent in Fig. 2b) [40]. The random coil-like conformation of PNIPAM chains leads to a broad size distribution and high PDI below T_{CP} [46]. It should be noted that PCHI is more extended at acidic condition because the protonation of amino groups causes intrachain charge repulsion. When heating over the T_{CP} , PNIPAM chain collapses from water-swollen coils to uniform aggregates, which consists of the hydrophobic core of PNIPAM and hydrophilic corona of CHI [40,43]. As a result, the distribution of the size became narrow with low value of PDI. Moreover, the inter-chain interaction of hydrophobic groups turns PCHI to aggregate in solution, which causes the light scattering effect (opaque appearance in Fig. 2b).

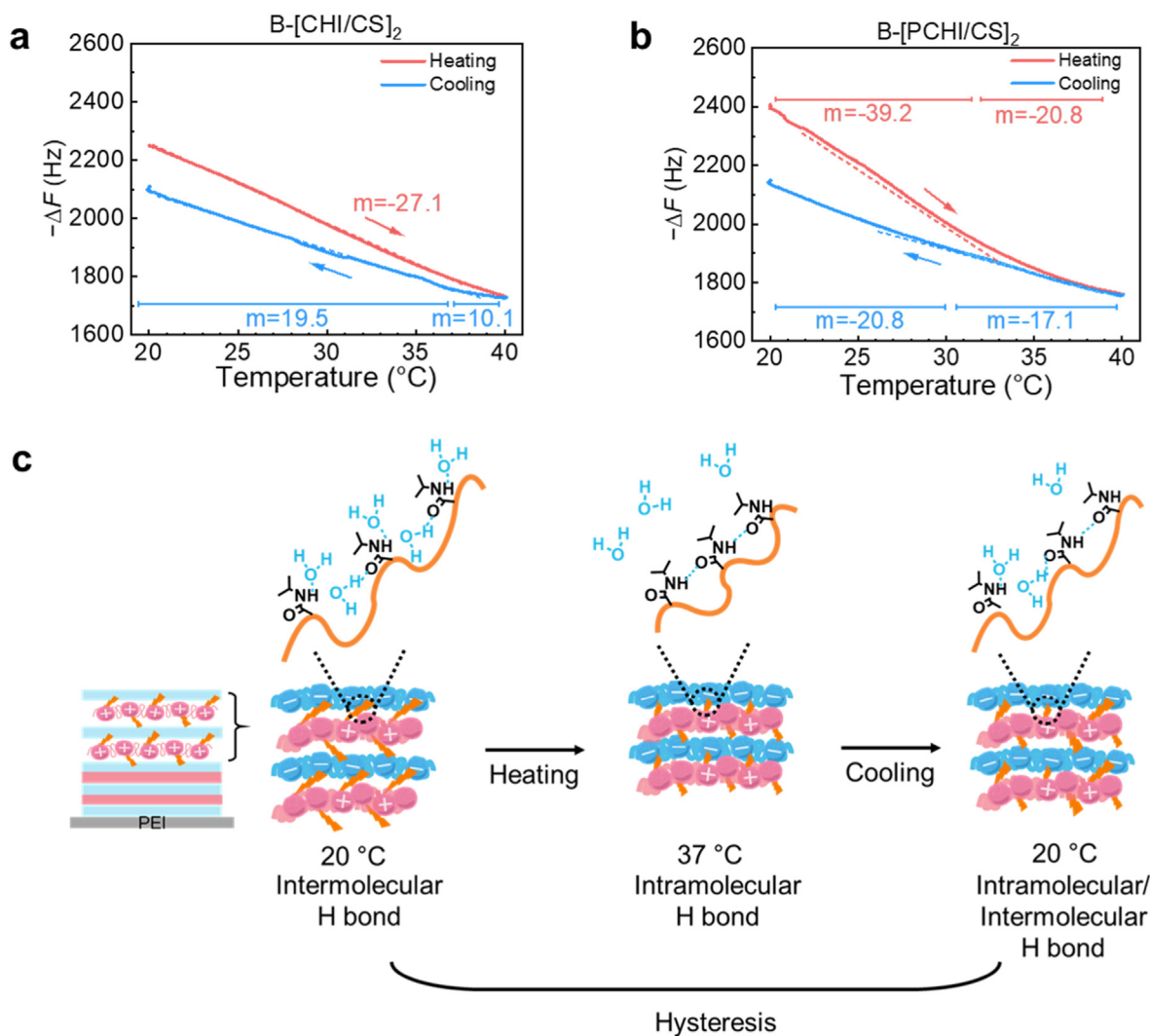


Fig. 4. Temperature dependence of frequency shift in the range of $20\text{--}40^\circ\text{C}$ for (a) B-[CHI/CS]₂ and (b) B-[PCHI/CS]₂ PEM rinsing with 150 mM NaCl buffer at pH 7.4. The term m refers to the slope of frequency shift during the temperature swap process. The red and blue lines indicate heating and cooling process, respectively. (c) Illustration represents the conformational change of the outermost layer at pH 7.4 related to hydrogen bond binding to PNIPAM from 7th to 10th layers during temperature cycle.

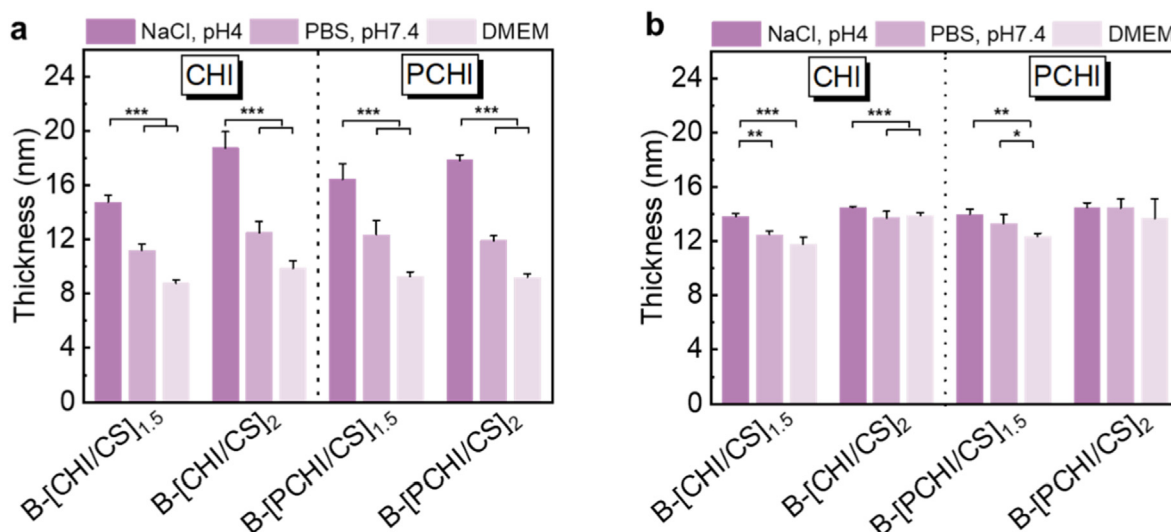


Fig. 5. Dry thickness of (a) uncrosslinked and (b) crosslinked of PEMs measured by ellipsometry after layer formation (deep pink), rinsing with PBS (pink) and with DMEM (light pink). B-[X/CS]_{1.5} represented PEM with terminal layer X = CHI or PCHI, while B-[X/CS]₂ referred to PEM with terminal layer CS. Data represent mean \pm SD, n = 4; *p \leq 0.05, **p \leq 0.01 and ***p \leq 0.001.

3.2. Multilayer formation

The layer growth of B-[CHI/CS]₂ and B-[PCHI/CS]₂ was monitored by the optical SPR method. Every layer deposition increased the angle shift corresponding to an increase in the adsorbed mass [47]. Fig. 3a shows an exponential growth behavior for both PEMs, which exhibited similar trends for the initial 6 basal layers based on the same type of PELs corresponding also to findings of other groups studying PEM formation from polysaccharides [48]. Starting from the 7th layer, the angle shift for B-[PCHI/CS] increased stronger for the following layers leading to 500° more than for B-[CHI/CS] at the end of complete PEM formation. Fig. S2a elaborates the normalized angle shift where the PCHI functional layer was added to compare the differences in both multilayers. A larger angle shift was detected after deposition of PCHI on the 7th layer, which caused an approximately doubled increased value compared to deposition of CHI owing to the higher molecular weight of PCHI similar to findings in other studies [30,49].

Different to SPR excluding solvent mass, QCM-D measurement was employed to determine the whole PEM including the 'wet mass' with the coupled water. According to Voigt equation (equation 1), the mass change is proportional to the negative frequency shift $-\Delta F$, reflecting the matter adsorbed on the surface of gold sensor. QCM-D provided similar results to SPR in terms of the adsorbed layer after the addition of PCHI as shown in Fig. 3b and Fig. S2b. More frequency change was detected for B-[PCHI/CS]₂ PEM, implicating larger quantity of adsorbed PELs plus intrinsic water than for B-[CHI/CS]₂ PEM, which is comparable to findings of SPR studies when water is not involved.

The damping shift measured by QCM-D was monitored to evaluate the mechanical properties of PEMs on the sensor surface after each adsorption step (Fig. 3c). The presence of damping shift ΔD indicated that the adsorbed PEM has viscoelastic properties with higher values associated to a softer film, whereas a dissipation is not seen in rigid films [48]. There was an increase in ΔD upon addition of the CS and CHI for the basal layer due to the existence of amino groups, sulfate groups, carboxyl groups, and hydroxyl groups to couple with more water and remained stable to the 6th layers, which seems to form intermingling layers. Strikingly, the measured ΔD increased sharply after PCHI adsorption from the 7th layer compared to CHI adsorption but decreased for the next CS deposition followed by similar trends for both PEMs until the process was completed. Our recent study on PCHI-containing multilayers using heparin as polyanion demonstrated that PNIPAM chains extended at 25 °C coupled more water molecules leading to the remarked swelling of the

PEM and increased ΔD [30]. It has been suggested in previous studies that the added PEL with smaller molecular weight displace small counter ions and water molecules to ionically pair with the prior adsorbed PEL, resulting in denser and more rigid multilayers [18,50]. The hydrogen bonds between PCHI and water were interrupted by following CS deposition bringing out a drop in dissipation values and de-swelling of the film [30]. Overall, despite potential steric hindrance effect of bulky PNIPAM as side chains on and the slightly reduced charge density of CHI, PCHI permits formation of PEM with CS.

Dry thickness could not be calculated with the results of SPR measurement due to unknown changes of refractive index during layer deposition. Hence, in order to know the effect of PNIPAM on water content of PEM, the hydration degree of the terminal CHI/PCHI and CS layers was calculated by comparison of the dry and hydrodynamic thickness obtained from ellipsometry and QCM-D, respectively (Table 2). In general, multilayers composed of polysaccharides or GAGs are soft and hydrated attributed to the presence of hydrophilic functional groups [51, 52]. Here Voigt model was applied to estimate the viscoelastic thickness of the PEMs. Indeed, the hydrodynamic thickness is larger than the dry thickness particularly around 7 nm more in B-[PCHI/CS] PEM, which shows the remarkable hydration degree of 25–28% compared to less than 20% in B-[CHI/CS] PEM. When applying the following CS layer, it caused dehydration in both PEM that is in line with the decreasing dampening shifts. Although the stretched conformation of PNIPAM coupled with more water below LCST seems to reduce the extent of dehydration in CS-terminated PEM, lesser ion pairing due to occupation of a part of amino groups in CHI should also be considered as a reason.

3.3. Temperature-dependent change of PEM mass

To study if conformational changes of PNIPAM bound to CHI during changes of temperature are related to swelling and shrinking of PEM, studies with QCM-D were carried out. Because the PEMs will be further studied in cell experiments, the measurements were carried out with NaCl solution at physiological pH 7.4 in the temperature range of 20–40 °C. Fig. 4a and b depict the temperature effect on the B-[CHI/CS]₂ and B-[PCHI/CS]₂ PEMs at pH 7.4. During the heating process, $-\Delta F$ decreased with the increasing temperature in both cases, indicating that the mass of the multilayer decreased on the resonator surface. Oppositely, $-\Delta F$ increased upon cooling process. It should be noted that the changes in viscosity and density of the running buffer with rising temperature contribute to the decrease in $-\Delta F$ [53]. Thus, NaCl buffer at 7.4 were

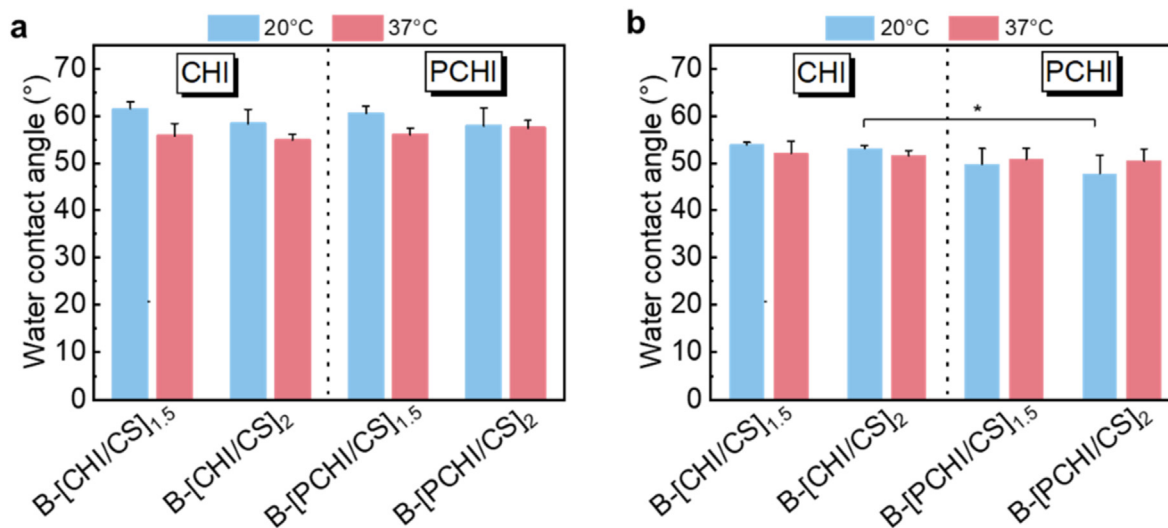


Fig. 6. Static water contact angle measurements of (a) uncrosslinked and (b) crosslinked PEMs with CHI/PCHI or CS terminal layer at 20 °C (blue bar) and 37 °C (red bar). Data represent mean \pm SD, $n = 5$; * $p \leq 0.05$.

applied to the bare gold sensor and ensured no substantial differences in $-\Delta F$ during temperature swaps in supporting information Fig. S3. It can be also assumed that no change in PEM mass adsorbed on the surface occurred during the experiment. Hence, the variation in the amount of water molecules present in the PEM must account for the change in ΔF [54]. Interestingly, when NaCl solution was flushed into the dry sensors to achieve a wet state at 20 °C in the beginning, higher $-\Delta F$ in B-[PCHI/CS]₂ PEM (200 Hz more) than B-[CHI/CS]₂ indicates higher water uptake due to the presence of PNIPAM. Another important observation is that the slope (m) of $-\Delta F$ was -39.2 below 31 °C and decreased to -20.8 above this temperature for B-[PCHI/CS]₂ PEM during heating cycle, while B-[CHI/CS]₂ PEM showed a constant slope of -27.1 in $-\Delta F$. The reason for the significantly steeper slope of B-[PCHI/CS]₂ PEM is that the water could be released during the heating process as PNIPAM gradually collapsed and underwent the coil-globular transition at 31 °C leading to the dehydration of the film. The slope became flatter above 31 °C because low quantity of water diffused out from PNIPAM film [54].

It was observed that both PEM systems showed two different paths during the cooling and heating cycles meaning a hysteresis effect. Upon heating, interdigitation between adjacent layers becomes stronger restricting the mobility of the polymer chains [33]. In other words, polymer layers undergo a rearrangement leading to the irreversible swelling after cooling [27,53]. In addition, hysteresis behavior is more obvious in B-[PCHI/CS]₂ PEM. The reason could be the additional hydrogen bonds formed between the collapsed PNIPAM chains upon heating across the coil-to-globular transition, consequently hindering the rehydration of the chains when cooling back to 20 °C (Fig. 4c) [55]. The behavior at pH 4 in Fig. S4 shows less pronounced temperature-induced change of PNIPAM in multilayer due to stronger ion pairing. Overall, despite less mobility of PNIPAM in the multilayer, the findings demonstrates that PEM with PCI as polycation respond to temperature.

3.4. Stability of PEMs

Since the integrity and poor cell adhesive surface of PEMs composed of polysaccharide PELs have been often a main issue under physiological conditions, covalent cross-linking was introduced between carboxylic groups of CS and amino groups of CHI or PCHI [22,30,56]. Fig. 5 depicts the measured dry thicknesses of PEMs by ellipsometry after PEM formation at pH 4 followed by rinsing with PBS and cell culture medium DMEM under physiological conditions. The overall average thickness of uncrosslinked PEMs was around 14.7–18.8 nm depending on the

terminal layer (Fig. 5a). After rinsing the PEMs with the two media at pH 7.4, the overall thickness was reduced to half probably due to the deprotonation of the amino groups of CHI ($pK_a \approx 6.5$) at pH 7.4 and the different ion content of medium (phosphate and other anions) resulted in a partial decomposition of PEMs [22]. On the other hand, crosslinked PEMs show a lower thickness about 13.9–14.5 nm (Fig. 5b). The thickness reductions after crosslinking indicates the formation of more compact PEM which have been also observed in other PEMs based on polysaccharides [22,57]. The difference of final average thickness between the crosslinked B-[CHI/CS] PEMs and B-[PCHI/CS] PEMs was not significant. In general, the PEM thickness increased as the molecular weight of the PEL increased due to more coiled conformation [15,57]. Nonetheless, the inclusion of the PCHI functional layer had no discernible effect on the thickness of our systems probably because the measurements were done under dehydrated states resulting in identical values to B-[CHI/CS] PEMs. Moreover, only a decrease of less than 2 nm of crosslinked PEMs after medium rinsing revealed that the formation of amide bonds strengthened the stability of PEMs despite the lower charge density of PCHI.

3.5. Temperature effect on surface wettability

Surface wettability is dependent on the surface composition and represents a prominent factor for the interaction of materials with proteins and cells [3,58]. Therefore, the wettability of the terminal layers with and without crosslinking was investigated by static water contact angle (WCA) measurement after rinsing PEM with PBS and DMEM (Fig. 6a and b). In general, CS coating (WCA $\sim 25^\circ - 30^\circ$) is supposed to increase the wettability of PEM different to the less wettable chitosan (WCA $\sim 90^\circ$) [59,60]. Here only slight differences in WCA between the alternating layers indicate the intermingling of PEL corresponding to QCM results and previous studies [17,61]. The average WCA in uncrosslinked PEMs was about $55-61^\circ$ compared to the noticeable 5° decrease of WCA after crosslinking. This is well in line with previous studies using carbodiimide chemistry for crosslinking multilayers composed of polysaccharides and related to the introduction of hydrophilic amides and increasing roughness [62,63].

On the other hand, regarding the surface wettability which could be affected by coil-to-globular transition of PNIPAM [64], the WCA of PEMs was studied at 20 °C and 37 °C. At 20 °C, the values of WCA were slightly lower for PCHI-PEMs than CHI-PEMs, owing to hydrophilic groups of PNIPAM in extended state coupling water molecules below the T_{CP} . At 37 °C, the values of WCA for uncrosslinked CHI-PEMs were found 5°

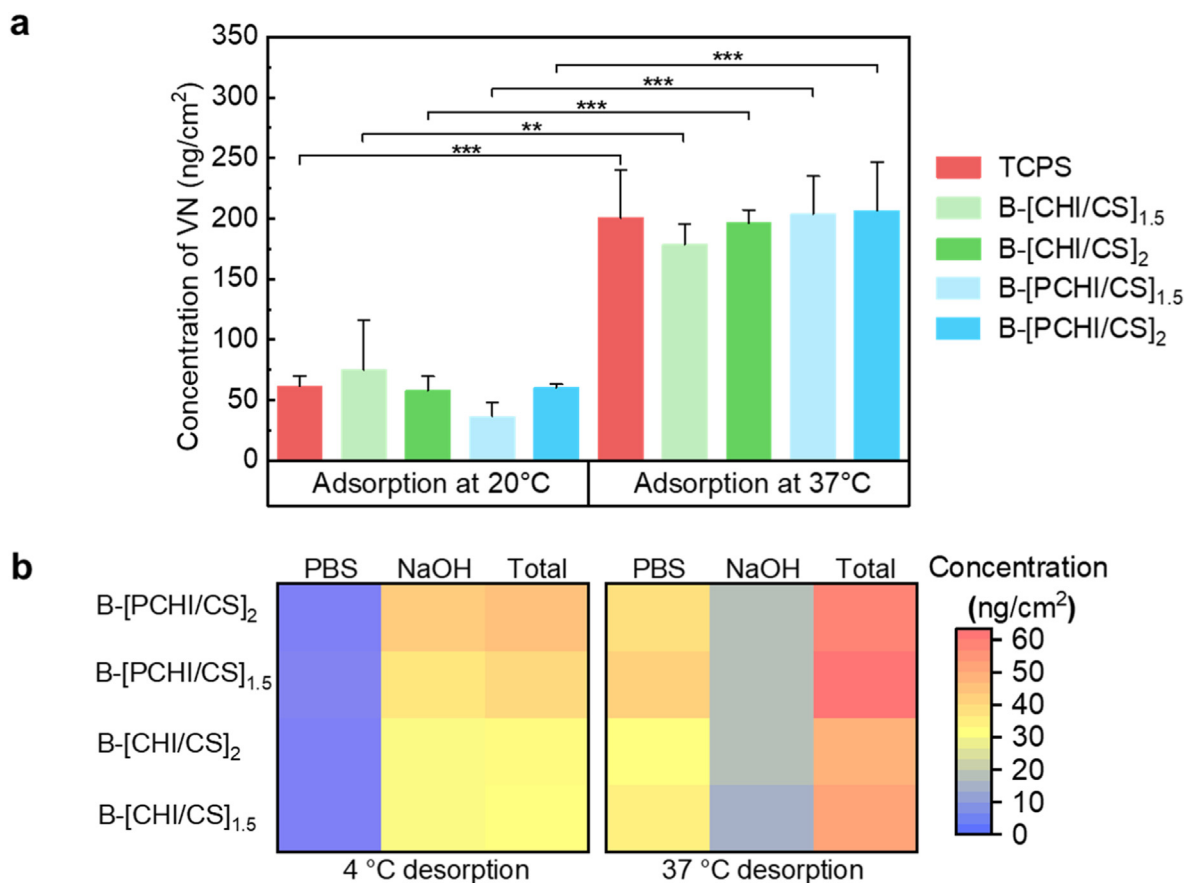


Fig. 7. (a) Temperature effect on vitronectin adsorption onto TCPS, and crosslinked PEMs with CHI/PCHI or CS terminal layer at 20 °C and 37 °C. $n = 4$, mean \pm SD, $**p \leq 0.01$ and $***p \leq 0.001$. (b) Temperature effect on vitronectin desorption at 4 °C and 37 °C from PEMs pre-adsorbed with vitronectin at 37 °C in PBS, followed by extraction in 200 mM NaOH for calculation of the cumulative amount of vitronectin.

lower than 20 °C. Although the same trend was also observed for uncrosslinked PCHI-PEMs, the change was rather limited ($<5^\circ$). In comparison, the WCA for crosslinked CHI-PEMs were lower at 37 °C than 20 °C but less than 5° difference. Specially, the WCA for crosslinked PCHI-PEMs were 1–3° higher at 37 °C than 20 °C, showing an opposite trend to uncrosslinked ones. The results reveal that the temperature has the impact on the surface wettability PCHI-PEM. The reason for lower WCA of uncrosslinked PEMs at higher temperature is probably attributed to thermally-induced rearrangement of PEMs and the decreased surface tension of water upon heating [27,65]. Even though the transition temperature of the uncrosslinked PCHI-PEM was found at 31 °C from QCM results, partial decomposition of uncrosslinked PEMs after rinsing at pH 7.4 did not show visible thermal sensibility related to PNIPAM in WCA. By contrast, the crosslinking seems to restrict some extent of rearrangement and decomposition of the polymers, which is correlated to lower WCA difference in crosslinked CHI-PEMs. Hence, with the enhanced stability, lower wettability in crosslinked PCHI-PEMs at high temperature is mainly contributed by domination of hydrophobic groups and collapse of PNIPAM [49].

3.6. FITC-labeled VN adsorption and desorption

Protein adsorption is dependent on surface properties of materials and related to adhesion of cells [10,66]. Vitronectin (VN) as a major cell adhesive protein secreted by cells or present in serum promotes cell adhesion and spreading even at very low concentrations [67]. Here FITC-VN adsorption was studied on TCPS as tissue culture related control and crosslinked PEMs at different temperatures at 20 (below T_{CP}) and 37 °C (above T_{CP}) shown in Fig. 7a. The values of adsorbed quantities of VN

are based on the calibration curve shown in Fig. S5a. Significantly higher amounts of adsorbed VN with more than 178 ng/cm² on all PEM were detected at 37 °C in comparison to only around 36–75 ng/cm² adsorbed at 20 °C. A similar trend of the temperature effect was also reported in other study but using ovalbumin on different PNIPAM-modified multi-layers [26,64]. According to the change of Gibbs free energy (ΔG), which is defined as

$$\Delta G = \Delta H - T\Delta S \quad (4)$$

(H : enthalpy; T : temperature; S : entropy), protein adsorption can occur if $\Delta G < 0$ [68]. When temperature is increased, entropy is gained by the release of adsorbed water molecules from the surface and structural rearrangements within the protein [68]. Thus, this thermodynamically driven process causes G of the system to decrease and promotes protein adsorption through hydrophobic interaction between the surface and protein. When integrating PNIPAM in PEMs, the amounts of VN were even greater at 37 °C than B-[CHI/CS] PEMs that seem to corroborate the findings of increased WCA for B-[PCHI/CS] PEM at 37 °C. Although the change in WCA is not significant, several reports claimed that the protein adsorption is mainly dependent on the hydrophobic interaction of dehydrated PNIPAM segments [27,64,69]. On the other hand, CS as GAG with sulfate groups has high affinity to the heparin-binding domain of VN [16]. As a result, higher amounts of VN adsorption were observed on the CS-terminated surfaces as shown in Fig. 7a as well.

Regarding the temperature effect on PNIPAM conformation, VN pre-adsorbed on PEM films at 37 °C was chosen to study the release/desorption of the protein at either 4 °C (below T_{CP}) or 37 °C (above T_{CP}), as shown in Fig. 7b. In the case of protein desorption in PBS during the first 24 h, obviously higher amounts of VN were released at 37 °C (>30

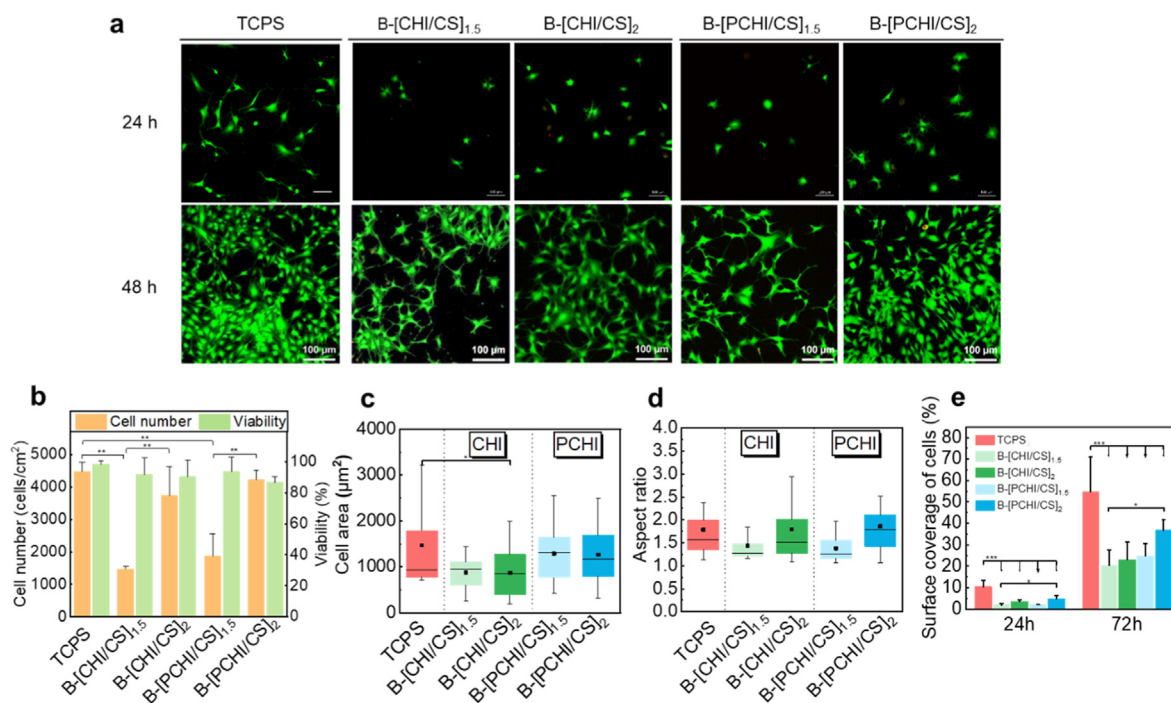


Fig. 8. Viability test and quantification of C3H10T1/2 cells on crosslinked multilayers with PCHI/CHI or CS terminal layers. (a) Confocal images of live (green) and dead (red) cells after 24 h and 72 h culture. Scale bar: 100 μm. Measurements of (b) cell number and viability and (c) cell area and aspect ratio after 24 h. Box plot with whisker represents the first and third quartiles, medians and means. Cell proliferation analyzed by surface coverage after 24 h and 72 h. Cell seeded on tissue culture polystyrene (TCPS) as a control; mean value ± SD with significance level of * $p < 0.05$ and *** $p < 0.001$.

ng/cm²) than 4 °C (<10 ng/cm²) from all PEMs. It has been already known that the enhanced protein mobility is kinetically driven by higher temperature [68]. To mobilize any remaining irreversibly adsorbed FITC-VN after the desorption step in PBS, a further extraction was done by NaOH hydrolysis as described in a previous work [70]. Here it was found that the extracted amount was 10 ng/cm² higher in samples processed at 4 °C compared to 37 °C. This is related to the higher amount of VN already released at 37 °C during incubation in PBS. Concerning the cell environment at 37 °C, it is essential to investigate the retention of VN on PEMs at this temperature. Slightly larger amount of VN with 10 ng/cm² was released from B-[PCHI/CS] PEMs, which might be linked to higher adsorption at 37 °C. Importantly, PEMs with CS terminal layers retained more VN on the surface owing to the specific interaction between CS and heparin-binding domain of VN [16]. Compared to almost 100% amount of VN desorbed from TCPS in Fig. S5b, the results suggest the PEM containing PNIPAM with CS terminal layer represents a promising bioactive surface.

3.7. Cytocompatibility studies

Cytocompatibility studies were done with the multipotent embryonic mouse fibroblast cell line that can differentiate into adipocytes, chondrocytes and osteocytes [71]. Since the crosslinking with EDC/NHS can exert some detrimental effects on cells, the cytotoxicity of both cross-linked B-[CHI/CS] and B-[PCHI/CS] PEMs was studied by quantification of the live (green fluorescence)/dead (red fluorescence) C3H10T1/2 cell staining after 24 h and 72 h cultivation (Fig. 8). TCPS as a cell-adhesive and biocompatible material was used as a reference. After 24 h, the CLSM images (Fig. 8a, upper row) show a slightly denser population of viable cells with only few dead cells on CS terminal layers particularly in the presence of PNIPAM. Cell viability is quantified in Fig. 8b showing more than 85% viable cells on PEMs with different terminal layers, while around 98% cells are alive on TCPS. The cell number and area of living cells were also quantified from the images. Notably, twice more cells adhered on CS terminal layers than on the CHI or PCHI terminal layers

(Fig. 8b). Likewise, cell spreading in terms of cell area and aspect ratio indicates that cells were larger and adopted a more elongated shape on the CS terminal layers (Fig. 8c and d). In particular, when cells were plated on PEMs with PCHI, higher cell number and spreading are observed, which are similar to cells cultured on TCPS. Further observations on cell proliferation after 72 h in Fig. 8a (lower row) shows that cells grow on all surfaces. The surface coverage of viable cells after 24 h and 72 h was evaluated from the images. Fig. 8e shows obviously the greatest cell expansion on the crosslinked B-[PCHI/CS]₂ PEM among the other PEMs after 72 h culture. The observation that a lower number of cells adhered on CHI or PCHI terminal layers during the first 24 h, was in line with little growth after 72 h.

Cell adhesion and subsequent spreading on biomaterials surfaces are crucial to govern further cell fates like survival, growth and differentiation [1]. Controlling surface properties like wettability of biocompatible materials is important for cell adhesion on the surfaces [2]. Here we confirmed by QCM and WCA studies that B-[PCHI/CS] PEM exhibiting a more dehydrated and less hydrophilic surfaces at 37 °C (above T_{CP}) promotes cell adhesion and growth due to hydrophobic interaction [10]. This is also related to higher protein adsorption on B-[PCHI/CS] PEM because VN is present in the serum of the culture medium and can support cell adhesion. Cell adhesion on the biomaterial surface is strongly dependent on the specific integrin-binding with adhesive proteins like VN, which could be attributed to ligation to $\alpha_v\beta_3$ integrin [9]. Other studies also found that the number of adhered cells and the rates of cell proliferation can be enhanced on surfaces modified with PNIPAM [72, 73]. Our previous study suggested that chemical crosslinking efficiently improves the stability of PEM and cell adhesion at physiological condition [30]. One of the reasons for increased cell adhesion and spreading on crosslinked PEM is their increased stiffness [74]. This enhances cell mechanosensing through integrins crucial for the contractile activity of actin-myosin cytoskeleton through RhoA/ROCK signaling pathway that promotes focal adhesion formation and spreading of the cells [75]. On the other hand, crosslinking stabilized the integrity of PEMs since CS remained tightly fixed in the terminal layer. CS with sulfate groups

provides the advantage of binding more adhesive proteins secreted by cells (e.g., fibronectin) and from serum (e.g., vitronectin) on the surface due to the specific interaction of protein heparin-binding domains promoting cell adhesion and growth through integrin ligation related to B-[X/CS]₂ [76]. On the other hand, B-[X/CS]_{1,5} with either CHI or PCHI as terminal layer does not possess such specific interaction with adhesive proteins like fibronectin and vitronectin which is related to lower cell adhesion. Thus, the results of cytocompatibility studies and cell adhesion/growth underline that the use of CS as biogenic polyanion is crucial for improvement of bioactivity of PCHI–PEMs.

4. Conclusion

A new kind of bioactive and thermoresponsive PEMs for cell culture substrates based on LbL sequential assembly of PCHI and CS is explored here. PCHI with low grafting density of PNIPAM can exhibit thermoresponsive properties and forms intermingling multilayer with CS at pH 4 despite its bulky structure at 25 °C (below T_{CP}). Covalent cross-linking is beneficial to effectively strengthen the stability of PEMs under physiological condition by the amide bond formation between amino groups of CHI and carboxylic groups of CS. Most importantly, not only less hydrophilicity of PNIPAM but also the terminal layer using CS for the cross-linked PCHI/CS–PEM play vital roles in promoting VN adsorption and stem cell adhesion at 37 °C. Overall, PEMs combined with PNIPAM and bioactive polysaccharides like CS suggest greater bioactivity, non-toxicity, and stimuli-responsivity for surface coatings. Hence, they are interesting for the application as culture substrata for stem and other cells during their in vitro culture.

CRedit authorship contribution statement

Yi-Tung Lu: Methodology, Validation, Investigation, Data curation, Writing – original draft. **Pei-Tzu Hung:** Investigation, Formal analysis, Data curation, Visualization, Writing – original draft. **Kui Zeng:** Methodology, Writing – review & editing. **Christian Woelk:** Methodology, Resources. **Bodo Fuhrmann:** Methodology, Resources. **Kai Zhang:** Conceptualization, Funding acquisition, Writing – review & editing. **Thomas Groth:** Supervision, Funding acquisition, Project administration, Conceptualization, Writing – review & editing.

Declaration of competing interest

The authors declare that they have no conflict of interest.

Acknowledgement

This work was funded by the International Graduate School AGRIP-OLY supported by the European Regional Development Fund (ERDF) and the Federal State Saxony-Anhalt, and Deutsche Forschungsgemeinschaft under grant agreements Gr 1290/12-1 and ZH 546/3-1. Dr. Kui Zeng thanks China Scholarship Council for his PhD grant.

Appendix A. Supplementary data

Supplementary data to this article can be found online at <https://doi.org/10.1016/j.smim.2022.11.008>.

References

- [1] O. Guillame-Gentil, O. Semenov, A.S. Roca, T. Groth, R. Zahn, J. Vörös, M. Zenobi-Wong, Engineering the extracellular environment: strategies for building 2D and 3D cellular structures, *Adv. Mater.* 22 (2010) 5443–5462.
- [2] M. Rahmati, E.A. Silva, J.E. Reseland, C.A. Heyward, H.J. Haugen, Biological responses to physicochemical properties of biomaterial surface, *Chem. Soc. Rev.* 49 (2020) 5178–5224.
- [3] G. Altankov, F. Grinnell, T. Groth, Studies on the biocompatibility of materials: fibroblast reorganization of substratum-bound fibronectin on surfaces varying in wettability, *J. Biomed. Mater. Res.* 30 (1996) 385–391.
- [4] M.S. Niepel, F. Almouhanna, B.K. Ekambaram, M. Menzel, A. Heilmann, T. Groth, Cross-linking multilayers of poly-L-lysine and hyaluronic acid: effect on mesenchymal stem cell behavior, *Int. J. Artif. Organs* 41 (2018) 223–235.
- [5] G. Altankov, K. Richau, T. Groth, The role of surface zeta potential and substratum chemistry for regulation of dermal fibroblasts interaction, *Mat.-wiss. u. Werkstofftech.* 34 (2003) 1120–1128.
- [6] M.S. Niepel, B. Fuhrmann, H.S. Leipner, T. Groth, Nanoscaled surface patterns influence adhesion and growth of human dermal fibroblasts, *Langmuir* 29 (2013) 13278–13290.
- [7] P. Esmailzadeh, T. Groth, Switchable and obedient interfacial properties that grant new biomedical applications, *ACS Appl. Mater. Interfaces* 11 (2019) 25637–25653.
- [8] K. Nagase, M. Yamato, H. Kanazawa, T. Okano, Poly(N-isopropylacrylamide)-based thermoresponsive surfaces provide new types of biomedical applications, *Biomaterials* 153 (2018) 27–48.
- [9] F. Doberenz, K. Zeng, C. Willems, K. Zhang, T. Groth, Thermoresponsive polymers and their biomedical application in tissue engineering - a review, *J. Mater. Chem. B* 8 (2020) 607–628.
- [10] M. Prawatborisut, S. Jiang, J. Oberländer, V. Mailänder, D. Crespy, K. Landfester, Modulating protein corona and materials–cell interactions with temperature-responsive materials, *Adv. Funct. Mater.* 32 (2022), 2106353.
- [11] X. Fan, M.E. Nash, A.V. Gorelov, F.P. Barry, G. Shaw, Y.A. Rochev, Thermoresponsive substrates used for the growth and controlled differentiation of human mesenchymal stem cells, *Macromol. Rapid Commun.* 36 (2015) 1897–1901.
- [12] I.-C. Peng, C.-C. Yeh, Y.-T. Lu, S. Muduli, Q.-D. Ling, A.A. Alarfaj, M.A. Munusamy, S.S. Kumar, K. Murugan, H. Lee, Y. Chang, A. Higuchi, Continuous harvest of stem cells via partial detachment from thermoresponsive nanobrush surfaces, *Biomaterials* 76 (2016) 76–86.
- [13] T.-C. Sung, H.C. Su, Q.-D. Ling, S.S. Kumar, Y. Chang, S.-T. Hsu, A. Higuchi, Efficient differentiation of human pluripotent stem cells into cardiomyocytes on cell sorting thermoresponsive surface, *Biomaterials* 253 (2020), 120060.
- [14] J. Borges, J.F. Mano, Molecular interactions driving the layer-by-layer assembly of multilayers, *Chem. Rev.* 114 (2014) 8883–8942.
- [15] J.M. Silva, R.L. Reis, J.F. Mano, Biomimetic extracellular environment based on natural Origin polyelectrolyte multilayers, *Small* 12 (2016) 4308–4342.
- [16] Y. Yang, Y.-T. Lu, K. Zeng, T. Heinze, T. Groth, K. Zhang, Recent progress on cellulose-based ionic compounds for biomaterials, *Adv. Mater.* 33 (2021), e2000717.
- [17] R. Anouz, A. Repanas, E. Schwarz, T. Groth, Novel surface coatings using oxidized glycosaminoglycans as delivery systems of bone morphogenetic protein 2 (BMP-2) for bone regeneration, *Macromol. Biosci.* 18 (2018), e1800283.
- [18] J.M. Silva, N. Georgi, R. Costa, P. Sher, R.L. Reis, C.A. van Blitterswijk, M. Karperien, J.F. Mano, Nanostructured 3D constructs based on chitosan and chondroitin sulphate multilayers for cartilage tissue engineering, *PLoS One* 8 (2013), e55451.
- [19] Y.A. Brito Barrera, G. Hause, M. Menzel, C.E.H. Schmelzer, E. Lehner, K. Mäder, C. Wölk, T. Groth, Engineering osteogenic microenvironments by combination of multilayers from collagen type I and chondroitin sulfate with novel cationic liposomes, *Mater. Today Bio* 7 (2020), 100071.
- [20] L. Marsili, M. Dal Bo, F. Berti, G. Toffoli, Chitosan-based biocompatible copolymers for thermoresponsive drug delivery systems: on the development of a standardization system, *Pharmaceutics* 13 (2021).
- [21] L. Richert, F. Boulmedais, P. Lavalle, J. Mutterer, E. Ferreux, G. Decher, P. Schaaf, J.-C. Voegel, C. Picart, Improvement of stability and cell adhesion properties of polyelectrolyte multilayer films by chemical cross-linking, *Biomacromolecules* 5 (2004) 284–294.
- [22] G. Apte, A. Repanas, C. Willems, A. Mujtaba, C.E.H. Schmelzer, A. Raichur, F. Syrowatka, T. Groth, Effect of different crosslinking strategies on physical properties and biocompatibility of freestanding multilayer films made of alginate and chitosan, *Macromol. Biosci.* 19 (2019), e1900181.
- [23] L. Xu, H. Wang, Z. Chu, L. Cai, H. Shi, C. Zhu, D. Pan, J. Pan, X. Fei, Y. Lei, Temperature-responsive multilayer films of micelle-based composites for controlled release of a third-generation EGFR inhibitor, *ACS Appl. Polym. Mater.* 2 (2020) 741–750.
- [24] L. Xu, X. Zhang, Z. Chu, H. Wang, Y. Li, X. Shen, L. Cai, H. Shi, C. Zhu, J. Pan, D. Pan, Temperature-responsive multilayer films based on block copolymer-coated silica nanoparticles for long-term release of Favipiravir, *ACS Appl. Nano Mater.* 4 (2021) 14014–14025.
- [25] T. Liao, M.D. Moussallem, J. Kim, J.B. Schlenoff, T. Ma, N-isopropylacrylamide-based thermoresponsive polyelectrolyte multilayer films for human mesenchymal stem cell expansion, *Biotechnol. Prog.* 26 (2010) 1705–1713.
- [26] A. Osypova, D. Magnin, P. Sibret, A. Aqil, C. Jérôme, C. Dupont-Gillain, C.-M. Pradier, S. Demoustier-Champagne, J. Landoulsi, Dual stimuli-responsive coating designed through layer-by-layer assembly of PAA-b-PNIPAM block copolymers for the control of protein adsorption, *Soft Matter* 11 (2015) 8154–8164.
- [27] A. Osypova, C.-A. Fustin, C.-M. Pradier, J. Landoulsi, S. Demoustier-Champagne, Factors impacting protein adsorption on layer-by-layer assembled stimuli-responsive thin films, *Eur. Polym. J.* 95 (2017) 195–206.
- [28] J.-P. Chen, T.-H. Cheng, Thermo-responsive chitosan-graft-poly(N-isopropylacrylamide) injectable hydrogel for cultivation of chondrocytes and mesenchymal cells, *Macromol. Biosci.* 6 (2006) 1026–1039.
- [29] S.B. Lee, D. in Ha, S.K. Cho, S.J. Kim, Y.M. Lee, Temperature/pH-sensitive comb-type graft hydrogels composed of chitosan and poly(N-isopropylacrylamide), *J. Appl. Polym. Sci.* 92 (2004) 2612–2620.
- [30] Y.-T. Lu, K. Zeng, B. Fuhrmann, C. Woelk, K. Zhang, T. Groth, Engineering of stable cross-linked multilayers based on thermo-responsive PNIPAM-grafted-chitosan/

- heparin to tailor their physicochemical properties and biocompatibility, *ACS Appl. Mater. Interfaces* 14 (2022) 29550–29562.
- [31] J. Giselbrecht, C. Janich, S.R. Pinnappireddy, G. Hause, U. Bakowsky, C. Wölk, A. Langner, Overcoming the polyclation dilemma - explorative studies to characterise the efficiency and biocompatibility of newly designed lipofection reagents, *Int. J. Pharm.* 541 (2018) 81–92.
- [32] J.A. Jaber, J.B. Schlenoff, Polyelectrolyte multilayers with reversible thermal responsivity, *Macromolecules* 38 (2005) 1300–1306.
- [33] K. Glinel, C. Déjugnat, M. Prevot, B. Schöler, M. Schönhoff, R.v. Klitzing, Responsive polyelectrolyte multilayers, *Colloids Surf. A Physicochem. Eng. Asp.* 303 (2007) 3–13.
- [34] R.B.M. Schasfoort, Chapter 1. Introduction to surface plasmon resonance, in: R.B.M. Schasfoort (Ed.), *Handbook of Surface Plasmon Resonance*, Royal Society of Chemistry, Cambridge, 2017, pp. 1–26.
- [35] G. Sauerbrey, Verwendung von Schwingquarzen zur Wgung dner Schichten und zur Mikrowgung, *Z. Phys.* 155 (1959) 206–222.
- [36] M.V. Voinova, M. Rodahl, M. Jonson, B. Kasemo, Viscoelastic acoustic response of layered polymer films at fluid-solid interfaces: continuum mechanics approach, *Phys. Scripta* 59 (1999) 391–396.
- [37] J.M. Silva, J.R. García, R.L. Reis, A.J. García, J.F. Mano, Tuning cell adhesive properties via layer-by-layer assembly of chitosan and alginate, *Acta Biomater.* 51 (2017) 279–293.
- [38] J. Almodóvar, L.W. Place, J. Gogolski, K. Erickson, M.J. Kipper, Layer-by-layer assembly of polysaccharide-based polyelectrolyte multilayers: a spectroscopic study of hydrophilicity, composition, and ion pairing, *Biomacromolecules* 12 (2011) 2755–2765.
- [39] J.D. Clogston, A.K. Patri, Zeta potential measurement, *Methods Mol. Biol.* 697 (2011) 63–70.
- [40] H. Bao, L. Li, W.C. Leong, L.H. Gan, Thermo-responsive association of chitosan-graft-poly(N-isopropylacrylamide) in aqueous solutions, *J. Phys. Chem. B* 114 (2010) 10666–10673.
- [41] L. Hou, P. Wu, LCST transition of PNIPAM-b-PVCL in water: cooperative aggregation of two distinct thermally responsive segments, *Soft Matter* 10 (2014) 3578–3586.
- [42] K. Zeng, F. Doberenz, Y.-T. Lu, J.P. Nong, S. Fischer, T. Groth, K. Zhang, Synthesis of thermoresponsive PNIPAM-grafted cellulose sulfates for bioactive multilayers via layer-by-layer technique, *ACS Appl. Mater. Interfaces* 14 (2022) 48384–48396.
- [43] C. Chen, M. Liu, C. Gao, S. Lü, J. Chen, X. Yu, E. Ding, C. Yu, J. Guo, G. Cui, A convenient way to synthesize comb-shaped chitosan-graft-poly (N-isopropylacrylamide) copolymer, *Carbohydr. Polym.* 92 (2013) 621–628.
- [44] Q. Zhang, C. Weber, U.S. Schubert, R. Hoogenboom, Thermoresponsive polymers with lower critical solution temperature: from fundamental aspects and measuring techniques to recommended turbidimetry conditions, *Mater. Horiz.* 4 (2017) 109–116.
- [45] M. Danaei, M. Dehghankhold, S. Ataei, F. Hasanzadeh Davarani, R. Javanmard, A. Dokhani, S. Khorasani, M.R. Mozafari, Impact of particle size and polydispersity index on the clinical applications of lipidic nanocarrier systems, *Pharmaceutics* 10 (2018).
- [46] X. Wang, X. Qiu, C. Wu, Comparison of the coil-to-globule and the globule-to-coil transitions of a single poly(N-isopropylacrylamide) homopolymer chain in water, *Macromolecules* 31 (1998) 2972–2976.
- [47] N. Aggarwal, N. Altgärde, S. Svedhem, K. Zhang, S. Fischer, T. Groth, Effect of molecular composition of heparin and cellulose sulfate on multilayer formation and cell response, *Langmuir* 29 (2013) 13853–13864.
- [48] C. Picart, Polyelectrolyte multilayer films: from physico-chemical properties to the control of cellular processes, *Curr. Med. Chem.* 15 (2008) 685–697.
- [49] G.V. Martins, J.F. Mano, N.M. Alves, Dual responsive nanostructured surfaces for biomedical applications, *Langmuir* 27 (2011) 8415–8423.
- [50] S.T. Dubas, J.B. Schlenoff, Factors controlling the growth of polyelectrolyte multilayers, *Macromolecules* 32 (1999) 8153–8160.
- [51] N. Aggarwal, N. Altgärde, S. Svedhem, G. Michanetzis, Y. Missirlis, T. Groth, Tuning cell adhesion and growth on biomimetic polyelectrolyte multilayers by variation of pH during layer-by-layer assembly, *Macromol. Biosci.* 13 (2013) 1327–1338.
- [52] M.P. Sousa, F. Cleymand, J.F. Mano, Elastic chitosan/chondroitin sulfate multilayer membranes, *Biomed. Mater.* 11 (2016), 35008.
- [53] M.A. Plunkett, Z. Wang, M.W. Rutland, D. Johannsmann, Adsorption of pNIPAM layers on hydrophobic gold surfaces, measured in situ by QCM and SPR, *Langmuir* 19 (2003) 6837–6844.
- [54] G. Zhang, Study on conformation change of thermally sensitive linear grafted poly(N-isopropylacrylamide) chains by quartz crystal microbalance, *Macromolecules* 37 (2004) 6553–6557.
- [55] M.H. Futscher, M. Philipp, P. Müller-Buschbaum, A. Schulte, The role of backbone hydration of poly(N-isopropyl acrylamide) across the volume phase transition compared to its monomer, *Sci. Rep.* 7 (2017), 17012.
- [56] G. Cavallaro, S. Micciulla, L. Chiappisi, G. Lazzara, Chitosan-based smart hybrid materials: a physico-chemical perspective, *J. Mater. Chem. B* 9 (2021) 594–611.
- [57] S. Amorim, I. Pashkuleva, C.A. Reis, R.L. Reis, R.A. Pires, Tunable layer-by-layer films containing hyaluronic acid and their interactions with CD44, *J. Mater. Chem. B* 8 (2020) 3880–3885.
- [58] Y. Arima, H. Iwata, Effect of wettability and surface functional groups on protein adsorption and cell adhesion using well-defined mixed self-assembled monolayers, *Biomaterials* 28 (2007) 3074–3082.
- [59] G. Zhou, H. Al-Khoury, T. Groth, Covalent immobilization of glycosaminoglycans to reduce the inflammatory effects of biomaterials, *Int. J. Artif. Organs* 39 (2016) 37–44.
- [60] S. Farris, L. Introzzi, P. Biagioni, T. Holz, A. Schiraldi, L. Piergiorganni, Wetting of biopolymer coatings: contact angle kinetics and image analysis investigation, *Langmuir* 27 (2011) 7563–7574.
- [61] N. Fauchoux, R. Schweiss, K. Lützw, C. Werner, T. Groth, Self-assembled monolayers with different terminating groups as model substrates for cell adhesion studies, *Biomaterials* 25 (2004) 2721–2730.
- [62] K. Ren, T. Crouzier, C. Roy, C. Picart, Polyelectrolyte multilayer films of controlled stiffness modulate myoblast cells differentiation, *Adv. Funct. Mater.* 18 (2008) 1378–1389.
- [63] G. Imbir, A. Mzyk, K. Trembecka-Wójciga, E. Jasek-Gajda, H. Plutecka, R. Schirhagl, R. Major, Polyelectrolyte multilayer films modification with Ag and rGO influences platelets activation and aggregate formation under in vitro blood flow, *Nanomaterials (Basel)* 10 (2020).
- [64] Y. Zhou, Y. Zheng, T. Wei, Y. Qu, Y. Wang, W. Zhan, Y. Zhang, G. Pan, D. Li, Q. Yu, H. Chen, Multistimulus responsive biointerfaces with switchable bioadhesion and surface functions, *ACS Appl. Mater. Interfaces* 12 (2020) 5447–5455.
- [65] H. Gr̄unewald, VonR.C. Weast, *Handbook of Chemistry and Physics*, vol. 52, The Chemical Rubber Co., Cleveland, Ohio/USA, 1972, pp. 445–446. Aufl., XXVII, 2313 S., geb. DM 99.80, *Angew. Chem.* 84 (1972).
- [66] T. Groth, G. Altankov, A. Kostadinova, N. Krasteva, W. Albrecht, D. Paul, Altered vitronectin receptor (v integrin) function in fibroblasts adhering on hydrophobic glass, *J. Biomed. Mater. Res.* 44 (1999) 341–351.
- [67] G. Toromanov, D. Gugutkov, J. Gustavsson, J. Planell, M. Salmerón-Sánchez, G. Altankov, Dynamic behavior of vitronectin at the cell-material interface, *ACS Biomater. Sci. Eng.* 1 (2015) 927–934.
- [68] I. Kiesel, M. Paulus, J. Nase, S. Tiemeyer, C. Sternemann, K. Ruster, F.J. Wirkert, K. Mende, T. Büning, M. Tolan, Temperature-driven adsorption and desorption of proteins at solid-liquid interfaces, *Langmuir* 30 (2014) 2077–2083.
- [69] J. Kobayashi, Y. Arisaka, N. Yui, Y. Akiyama, M. Yamato, T. Okano, Effect of temperature changes on serum protein adsorption on thermoresponsive cell-culture surfaces monitored by a quartz crystal microbalance with dissipation, *Int. J. Mol. Sci.* 19 (2018).
- [70] N.M. Coelho, C. González-García, J.A. Planell, M. Salmerón-Sánchez, G. Altankov, Different assembly of type IV collagen on hydrophilic and hydrophobic substrata alters endothelial cells interaction, *Eur. Cell. Mater.* 19 (2010) 262–272.
- [71] H. Kindi, M. Menzel, A. Heilmann, C.E.H. Schmelzer, M. Herzberg, B. Fuhrmann, G. Gallego-Ferrer, T. Groth, Effect of metal ions on the physical properties of multilayers from hyaluronan and chitosan, and the adhesion, growth and adipogenic differentiation of multipotent mouse fibroblasts, *Soft Matter* 17 (2021) 8394–8410.
- [72] V. Capella, R.E. Rivero, A.C. Liaudat, L.E. Ibarra, D.A. Roma, F. Alustiza, F. Mañas, C.A. Barbero, P. Bosch, C.R. Rivarola, N. Rodríguez, Cytotoxicity and bioadhesive properties of poly-N-isopropylacrylamide hydrogel, *Heliyon* 5 (2019), e01474.
- [73] E. Psarra, U. König, Y. Ueda, C. Bellmann, A. Janke, E. Bittrich, K.-J. Eichhorn, P. Uhlmann, Nanostructured biointerfaces: nanoarchitectonics of thermoresponsive polymer brushes impact protein adsorption and cell adhesion, *ACS Appl. Mater. Interfaces* 7 (2015) 12516–12529.
- [74] M.S. Niepel, B.K. Ekambaram, C.E.H. Schmelzer, T. Groth, Polyelectrolyte multilayers of poly (l-lysine) and hyaluronic acid on nanostructured surfaces affect stem cell response, *Nanoscale* 11 (2019) 2878–2891.
- [75] L. Yu, Y. Hou, W. Xie, J.L.C. Camacho, C. Cheng, A. Holle, J. Young, B. Trappmann, W. Zhao, M.F. Melzig, E.A. Cavalcanti-Adam, C. Zhao, J.P. Spatz, Q. Wei, R. Haag, Ligand diffusion enables force-independent cell adhesion via activating $\alpha 5\beta 1$ integrin and initiating rac and RhoA signaling, *Adv. Mater.* 32 (2020), 2002566.
- [76] A. Köwitsch, G. Zhou, T. Groth, Medical application of glycosaminoglycans: a review, *J. Tissue Eng. Regen. Med.* 12 (2018) e23–e41.